Optics Letters

Controlling an optical vortex array from a vortex phase plate, mode converter, and spatial light modulator

T. D. Huang and T. H. Lu*

Department of Physics, National Taiwan Normal University, Taipei 11677, Taiwan
**Corresponding author: thlu@ntnu.edu.tw*

Received 2 July 2019; accepted 2 July 2019; posted 9 July 2019 (Doc. ID 371442); published 6 August 2019

In this Letter, we propose a convenient method of generating an optical vortex (OV) array, in which the size and quantity can be controlled by employing vortex phase plates, a mode converter, and a spatial light modulator into a simple optical system. Different sizes of OV arrays are generated from the superposition of crossed Hermite–Gaussian (HG) modes possessing equal or unequal orders and mutually orthogonal circular polarizations. We experimentally and theoretically demonstrate a series of vector superposed optical fields. Here the sizes of the OV arrays, as well as the quantities of OVs, are defined in terms of specific sets of HG bases. Our results indicate that a simple setup can be used to effectively generate and control OVs and OV arrays.

https://doi.org/10.1364/OL.44.003917

First introduced in 1992 by Allen *et al.* [1], light with orbital angular momentum (OAM), also called the Laguerre–Gaussian (LG) mode, possesses an OAM of $\ell\hbar$ per photon. Its twisted phase wavefront is a manifestation of the azimuthal phase term in its wavefunction, while the phase singularities along the beam axis are defined as the optical vortices (OVs). Thus, OAM light is attractive to numerous studies such as optical cryptography [2,3], optical tweezers [4,5], and optical testing [6]. In general, there are several direct approaches to generate the OAM light: these include the use of spatial light modulators [7–9], laser resonators [10,11], and spiral phase plates [12,13]. Mode converters [14], on the other hand, provide a passive way to generate OAM light by transforming Hermite–Gaussian (HG) modes into LG modes. In recent years, the vector OAM beam has also attracted much attention in the fields of optical communication [15–17] and optical entanglement [18,19] due to an extra degree of freedom provided by its space-inhomogeneous polarization. Common methods of generating vector beams include a Sagnac or a Mach–Zehnder interferometric configuration, among others [20]; however, recently, more convenient and highly efficient generation processes have already been used [21]. Moreover, a metasurface, called the q-plate [22,23] or vortex phase plate (VPP), provides an extra convenient way of generating and realizing vector OAM beams [24].

In this Letter, we propose a convenient and powerful method to produce and control the OV array of the vector superposed optical field, which is composed of different orders of crossed HG bases with opposite helicity of circular polarization. The VPP, which does not require a voltage, is used to produce the vector LG beam from an incident linearly polarized light. This vector beam is composed of two opposite orders of the LG beam with orthogonal circular polarization. Meanwhile, the bases can be transformed from LG beams into crossed HG beams with orthogonal circular polarization by using a mode converter. The SLM provides an extra degree of freedom to increase and control the order of the bases in the vector superposed optical field, which can induce OVs of different sizes and quantities. The position of each OV has been calculated, and the variable size of the OV array has also been discussed in calculations. All experimental results are consistent with the theoretical analysis.

VPPs are made up of a layer of liquid crystal film which is sandwiched by two glasses. The fast-axis orientation distribution of the liquid crystal can be described by the relation: $\alpha(r,\phi) = m \times \phi + \alpha_0$, where r is the radial coordinate, ϕ is the azimuthal coordinate, and α_0 is a constant angle specifying the initial orientation of the liquid crystal along the x-axis. The parameter m determines the order of the VPP and is related to the topological charge of the LG beam, as well as the distribution of its space-inhomogeneous polarization. The LG mode of topological charge m ($-m$) with the right (left) circular polarization can be generated when a left (right) circularly polarized light impinged into the VPP. The transformational relation of the above system can be written as

$$|E_{\text{out}}\rangle = e^{im\phi}|R\rangle\langle L|E_{\text{in}}\rangle + e^{-im\phi}|L\rangle\langle R|E_{\text{in}}\rangle. \quad (1)$$

Furthermore, when the incident light is horizontally (linear) polarized ($|H\rangle = 1/\sqrt{2}(\psi_{0,0}^{(\text{LG})}|R\rangle + \psi_{0,0}^{(\text{LG})}|L\rangle)$), Eq. (1) can be rewritten as

$$|E_{\text{out}}\rangle = 1/\sqrt{2}(\psi_{0,-m}^{(\text{LG})}|L\rangle + \psi_{0,m}^{(\text{LG})}|R\rangle), \quad (2)$$

where $\psi_{p,\ell}^{(\text{LG})}$ represents the LG mode with radial index p and topological charge ℓ, and the parameter m corresponds to the

order of the VPP. Thus, vector LG beams can be decomposed into two bases, $\psi^{(LG)}_{0,-m}|L\rangle$ and $\psi^{(LG)}_{0,m}|R\rangle$. In this experiment, VPPs with $m = 1$ and 2 are used. To visually distinguish the bases of the LG modes generated from the VPP of different orders, a mode converter is applied to transform the transverse laser mode from LG modes into HG modes. A mode converter is composed of two identical cylindrical lenses with focal length f, separated by $\sqrt{2}f$. The transformational relation between $\psi^{(HG)}_{m,n}$ and $\psi^{(LG)}_{p,\ell}$ is stated by the equations $p = \min(m, n)$ and $\ell = n - m$. Allen *et al.* [25] reported a matrix formulation for light beams possessing spin and OAM. According to the concept, an LG mode can be transformed into a single HG mode, if the axis of the mode converter is rotated at an angle of 45° or −45°. On the other hand, Lin *et al.* [26] declared that crossed HG modes possess various extra relative phase shifts δ when the mode converter is rotated at different angles. Figures 1(a) and 1(b) are an experimental setup, which shows a diode-pumped solid-state laser, with a wavelength of 532 nm and output power of 20 mW, incident to VPPs of $m = 1$ and 2. The setup also includes a mode converter rotated at −45°. According to Eq. (2), the vector superposed optical field is described by two LG bases with opposite topological charges and helicities of circular polarization, and is transformed into two crossed HG modes with opposite circular polarization when the mode converter is utilized. By considering the mode transformation, and using equations $|L\rangle = 1/\sqrt{2}(\hat{x} - i\hat{y})$ and $|R\rangle = 1/\sqrt{2}(\hat{x} + i\hat{y})$, Eq. (2) can be written as

$$|E_{\text{out}}\rangle = 1/2[(\psi^{(HG)}_{m,0} + e^{i\delta}\psi^{(HG)}_{0,m})\hat{x} + i(\psi^{(HG)}_{0,m} - e^{i\delta}\psi^{(HG)}_{m,0})\hat{y}], \tag{3}$$

where $\psi^{(HG)}_{m,n}$ represents the HG mode with the order m in the x-direction and order n in the y-direction; δ represents the extra relative phase shift generated from the mode converter. Thus, each combination of HG modes in the x- and y-direction can easily be comprehended when the circularly polarized bases are transformed into linearly polarized bases. Figure 2(a) shows the intensity profile of an incident linearly polarized light impinged onto a VPP with $m = 1$ and passed through a mode converter.

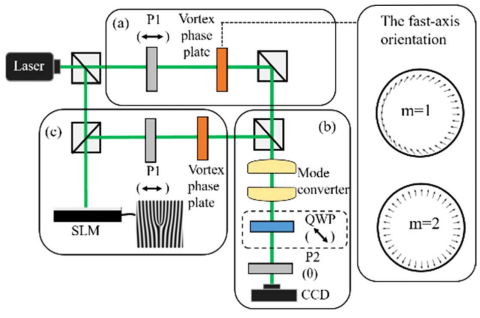

Fig. 1. (a) Experimental setup composed of a polarizer P1 and a VPP which are applied to generate a vector superposed LG beam. Different VPPs have different fast-axis orientation distributions. (b) Mode converter combined with a QWP and a polarizer P2 used either to transform LG modes into HG modes or to analyze mode bases and polarization distributions. (c) Combination of a VPP and a higher-order LG mode generated by a computer-generated hologram on the SLM; P1 is utilized to manipulate the incident polarization state. All experimental results are recorded by the CCD.

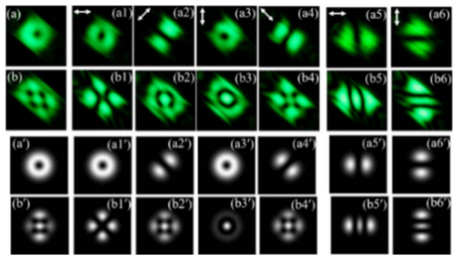

Fig. 2. (a)–(b) Experimental intensities of an incident linearly polarized light that has passed through a VPP with $m = 1$ and 2, respectively, and a mode converter. (a1)–(a4) and (b1)–(b4) Corresponding spatial intensities of the optical fields in Figs. 2(a) and 2(b) at different angles of P2, respectively. (a5)–(a6) and (b5)–(b6) HG bases $\psi^{(HG)}_{1,0}|L\rangle$, $\psi^{(HG)}_{0,1}|R\rangle$ and $\psi^{(HG)}_{2,0}|L\rangle$, and $\psi^{(HG)}_{0,2}|R\rangle$, respectively, analyzed by a combination of a QWP with a fast axis set at −45° and vertically and horizontally oriented P2. The white arrows represent the angles of P2. The theoretical results, shown in the third and fourth rows, correspond well to the experimental results.

Figures 2(a1)–2(a4) indicate the polarization-resolved spatial intensities of the optical field in Figure 2(a) via the polarizer (P2), and the results clearly show that the superposed optical modes possess space-inhomogeneous polarization distribution. Figures 2(a5) and 2(a6), meanwhile, denote the optical field that has passed through a combination of a quarter-wave plates (QWPs) at −45° orientation and a polarizer at 0° and 90° orientations. The results, taken after varying the horizontal and vertical polarizer orientations, can be described by the beam's left and right circular polarization bases, represented as $\psi^{(HG)}_{1,0}|L\rangle$ and $\psi^{(HG)}_{0,1}|R\rangle$, respectively. Figure 2(b) shows the intensity profile of an incident linearly polarized light impinged onto a VPP with $m = 2$ and passed through a mode converter.

Figures 2(b1)–2(b4), which display the polarization-resolved spatial intensities of the optical field in Fig. 2(b), indicate that the optical field possesses a more complicated space-inhomogeneous polarization distribution. The two orthogonal circularly polarized bases $\psi^{(HG)}_{2,0}|L\rangle$ and $\psi^{(HG)}_{0,2}|R\rangle$ are analyzed in Figs. 2(b5) and 2(b6) by using a combination of a QWP and a polarizer. The mode converter induces relative phase shifts $\delta = \pi/2$ and $\delta = \pi$ in the experimental results shown in Figs. 2(a) and 2(b). The numerical results, calculated using Eq. (3) and are shown in the third and fourth row of Fig. 2, have good agreement with the experimental results. On the other hand, the SLM was employed to generate different linearly polarized $\psi^{(LG)}_{0,\ell}$ modes of higher topological charge (ℓ) which were passed through the VPP and the mode converter in order to increase and control the order of the bases of the vector superposed HG modes. Figure 1(c) depicts the experimental setup of an incident diode-pumped green laser directed onto a reflective phase-only 1920 × 1080 pixel SLM with a pixel pitch of 8 μm. The grating phase pattern of the desired mode is displayed onto the SLM, and the iris is then used to select the desired order of the LG mode for the diffracted optical field. The selected LG mode impinged into a polarizer and a VPP of order m, and the vector superposed optical field is afterward transformed by the mode converter. Following Eqs. (2) and (3), the vector superposed optical field can be represented as

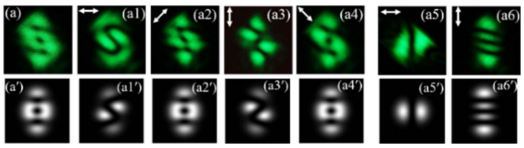

Fig. 3. (a) Experimental intensity profile of the $\psi_{0,1}^{(\mathrm{LG})}|H\rangle$ mode that has passed through a VPP of $m = 2$ and a mode converter. (a1)–(a4) Corresponding spatial intensities of the optical field in (a) at different angles of P2. (a5)–(a6) HG bases, $\psi_{1,0}^{(\mathrm{HG})}|L\rangle$ and $\psi_{0,3}^{(\mathrm{HG})}|R\rangle$, respectively, analyzed by a combination of a QWP with a fast axis set at −45° and vertically and horizontally oriented P2. The white arrows represent the different angles of P2. The theoretical results, shown in the second row, are consistent with the experimental results.

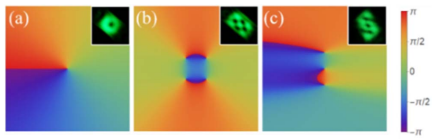

Fig. 4. (a) Phase distribution corresponds to the inset and Fig. 2(a); there is an OV located at (0, 0). The size of the OV array is 1 × 1. (b) Phase diagram corresponds to the inset and Fig. 2(b); there are four OVs which are located at $(\omega_0/2, \omega_0/2)$, $(-\omega_0/2, \omega_0/2)$, $(\omega_0/2, -\omega_0/2)$, and $(-\omega_0/2, -\omega_0/2)$. The size of the OV array is 2 × 2. (c) Phase diagram corresponds to the inset and Fig. 3(a); there are three OVs which are located at (0, 0), $(0, \sqrt{3}\omega_0/2)$, and $(0, -\sqrt{3}\omega_0/2)$. The size of the OV array is 3 × 1.

$$|E_{\mathrm{out}}\rangle = \psi_{|\ell-m|,0}^{(\mathrm{HG})}|L\rangle + e^{i\delta}\psi_{0,|\ell+m|}^{(\mathrm{HG})}|R\rangle. \tag{4}$$

The two orthogonal HG bases can be achieved by satisfying the condition $|\ell| < m$. When an incident $\psi_{0,\ell}^{(\mathrm{LG})}$ is applied onto the VPP of order m and onto the mode converter, the order of the two HG bases is transformed, specifically, from two orthogonal HG modes with the same order m [Eq. (3)] into two orthogonal HG modes with orders $|\ell - m|$ and $|\ell + m|$. Figure 3(a) shows a linearly polarized $\psi_{0,1}^{(\mathrm{LG})}$ mode applied onto a VPP of $m = 2$ and passed through the mode converter.

The intensity profile clearly reveals that the superposed optical field is composed of two HG bases with unequal orders. Figures 3(a1)–3(a4) presented the polarization-resolved spatial intensities of the optical beam in Fig. 3(a) via P2. The vector superposed beam generated from the optical system with a higher order of LG mode demonstrates the diversity of the polarization-resolved patterns. Figures 3(a5) and 3(a6) show that the two orthogonal bases are $\psi_{0,3}^{(\mathrm{HG})}|R\rangle$ and $\psi_{1,0}^{(\mathrm{HG})}|L\rangle$; the superposed HG modes passed through the combination of a QWP with −45° orientation and a polarizer with vertical and horizontal orientations. Consequently, the SLM provides an extra degree of freedom to control the order of the bases of the two HG modes in the vector superposed optical field. All experimental results have good agreement with the numerical results, as shown in the second row of Fig. 3. It is worth mentioning that the OV of the $m \times n$ array exists in the vector superposed optical field. The OV is defined as the phase singularity, where both the real and imaginary parts of the wavefunction are equal to zero. Moreover, the phase singularity usually generates a null intensity in the intensity profile. Chu *et al.* [27] demonstrated an OV array that was generated from an end-pumped solid-state laser using an unbalanced Mach–Zehnder interferometer and a rotated Dove prism. A $\pi/2$ phase difference was provided between the two sub-beams, contributing an extra i coefficient to the superposed beam. Furthermore, Lin *et al.* [26] generated a square OV array from an end-pumped solid-state laser using a mode converter, which also provides extra phase shifts. Thus, extra phase shifts are necessary for generating a laser with an $m \times n$ OV array. According to Eq. (3), the coefficient i is provided by the imaginary components of the left and right circular polarizations. Following the experimental intensities, the positions of the OVs do not change, even after varying the polarizer angles. Figures 4(a)–4(c) demonstrate the phase distributions corresponding to the experimental intensity results of Figs. 2(a), 2(b), and 3(a), which are shown in the insets. The phase diagram is drawn in the Cartesian coordinate with the origin defined at the center of the diagram. The size of the OV array and the quantity of OV depend on the bases of the HG modes. Moreover, by solving the positions of the OVs using their respective wavefunctions, it was found that an OV is located at $(x, y) = (0, 0)$ in Fig. 2(a); four OVs are located at $(x, y) = (\omega_0/2, \omega_0/2)$, $(\omega_0/2, -\omega_0/2)$, $(-\omega_0/2, \omega_0/2)$, and $(-\omega_0/2, -\omega_0/2)$ in Fig. 2(b); and three OVs are located at $(x, y) = (0, 0)$, $(0, \sqrt{3}\omega_0/2)$ and $(0, -\sqrt{3}\omega_0/2)$ in Fig. 3(a). The sizes of the OV arrays in Fig. 4(a)–4(c) are 1 × 1, 2 × 2, and 3 × 1, respectively. All solutions are described in terms of ω_0, which is the beam waist of the laser. Furthermore, the size of the OV array and the quantity of OV can further be controlled by utilizing different categories of incident transverse laser modes interacting with a VPP of $m = 2$ and a mode converter. First, the simulated linearly polarized standing-wave LG modes, $\psi_{0,4}^{(\mathrm{LG})} + \psi_{0,-4}^{(\mathrm{LG})}$ and $\psi_{0,10}^{(\mathrm{LG})} + \psi_{0,-10}^{(\mathrm{LG})}$, are treated as the transverse modes, as shown in Figs. 5(a) and 5(b). Following Eqs. (3) and (4), the calculated intensities of the vector superposed optical field in terms of the HG bases and the calculated phase distributions are shown in Figs. 5. (a′)–5(b′) and 5(a″)–5(b″), respectively. The calculated intensities of the superposed

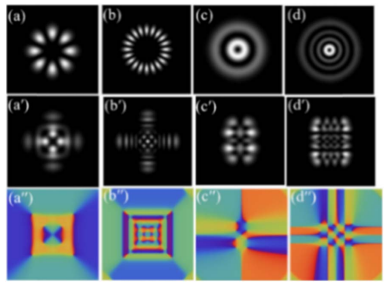

Fig. 5. (a)–(d) Simulated transverse mode of $\psi_{0,4}^{(\mathrm{LG})} + \psi_{0,-4}^{(\mathrm{LG})}$, $\psi_{0,10}^{(\mathrm{LG})} + \psi_{0,-10}^{(\mathrm{LG})}$, $\psi_{1,1}^{(\mathrm{LG})}$ and $\psi_{3,1}^{(\mathrm{LG})}$, respectively. All modes interact with the VPP of $m = 2$ and with the mode converter. (a′)–(d′) Calculated superposed optical fields in terms of HG bases corresponding to (a)–(d). (a″)–(d″) Calculated phase distributions for (a′)–(d′), indicating the quantity of OV to be 8, 20, 9, and 33, respectively; the alignment of the OV array is analyzed as 2 × (2 × 2), 5 × (2 × 2), 4 × 2 + 1 × 1, and 6 × 4 + 3 × 3, accordingly.

optical field can be described by the $1/2[(\psi_{0,6}^{(LG)}+\psi_{0,-2}^{(LG)})\hat{x}+i\hat{y}(\psi_{0,2}^{(LG)}+\psi_{0,-6}^{(LG)})]$ and $1/2[(\psi_{0,12}^{(LG)}+\psi_{8,0}^{(LG)})\hat{x}+i\hat{y}(\psi_{0,8}^{(LG)}+\psi_{12,0}^{(LG)})]$, respectively. In the case of the incident standing-wave LG modes, the quantity of LG bases has increased from one LG basis to two LG bases of unequal orders, in each x- or y-direction, expanding the diversity of OV array. The phase distributions presented in Figs. 5 (a′′) and 5(b′′) show that the OV array is composed of many sets of 2×2 OV square arrays (quantity of OV). Specifically, there are two sets of 2×2 arrays (8 OVs) in Fig. 5(a′′), and 5 sets of 2×2 arrays 20) OVs) in Fig. 5(b′′). The N sets of 2×2 arrays and the 4N OVs are related to the standing-wave LG modes $\psi_{0,N\times 2}^{(LG)}+\psi_{0,-N\times 2}^{(LG)}$. Furthermore, the alignment of the OV array and the quantity of OV with respect to the odd-ordered standing-wave LG mode, $\psi_{0,2N+3}^{(LG)}+\psi_{0,-2N-3}^{(LG)}$, are described by $5\times 1+N\times(2\times 2)$ and $4N+5$, respectively. Secondly, higher p order $\psi_{p,\ell}^{(LG)}$ mode was used as an incident light to the VPP with $m=2$ and to the mode converter, which provides an extra degree of freedom to generate two-dimensional (2D) HG modes. The $\psi_{1,1}^{(LG)}$ and $\psi_{3,1}^{(LG)}$ modes are treated as incident transverse modes and are shown in Figs. 5(c) and 5(d). The calculated intensities of the vector superposed optical field in terms of HG bases are presented in Figs. 5(c′) and 5(d′), which are described by $\psi_{1,4}^{(HG)}|R\rangle+\psi_{2,1}^{(HG)}|L\rangle$ and $\psi_{3,6}^{(HG)}|R\rangle+\psi_{4,3}^{(HG)}|L\rangle$, respectively. The results have clearly demonstrated that the vector superposed field is composed of two 2D HG bases with orthogonal circular polarization. Figures 5(c′′) and 5(d′′) display the calculated phase distributions of the vector superposed fields showing the presence of 9 vortices and 33 vortices, respectively. Moreover, the alignment of the OV array is analyzed as $4\times 2+1\times 1$ and $6\times 4+3\times 3$, respectively. Notably, the general expression for the alignment of OV array and quantity of OV is $n_1\times m_2+n_2\times m_1$ for $\psi_{m_1,n_1}^{(HG)}|R\rangle+\psi_{m_2,n_2}^{(HG)}|L\rangle$.

In conclusion, we proposed a convenient and powerful method to control the size of the OV array and the quantity of OVs. VPPs of $m=1$ and 2 have been utilized to generate the vector LG beam using an incident linearly polarized light, which is composed of two LG bases with the orthogonal order and helicity of circular polarization. To visually distinguish the superposed optical field of LG bases, a mode converter is applied to transform the two bases of LG modes into two crossed HG modes. Moreover, each basis is analyzed by a combination of QWP and polarizer. The SLM provides an extra degree of freedom to control the HG bases of vector superposed field. Furthermore, simulations show that the quantity of OV and the size of the OV array can be further controlled by utilizing the standing-wave and higher p order LG modes, respectively. Finally, the general expressions of the OV array have been provided to conveniently control the OV array and the quantity of OV. This approach is expected to create various sizes of OV arrays and paves the way for quantum entanglement and quantum communications.

Funding. Ministry of Science and Technology, Taiwan (MOST) (MOST 107-2112-M-003-012).

REFERENCES

1. L. Allen, M. W. Beijersbergen, R. J. Spreeuw, and J. P. Woerdman, Phys. Rev. A **45**, 8185 (1992).
2. M. Mirhosseini, O. S. Magaña-Loaiza, M. N. O'Sullivan, B. Rodenburg, M. Malik, M. P. Lavery, M. J. Padgett, D. J. Gauthier, and R. W. Boyd, New J. Phys. **17**, 033033 (2015).
3. A. Sit, F. Bouchard, R. Fickler, J. Gagnon-Bischoff, H. Larocque, K. Heshami, D. Elser, C. Peuntinger, K. Günthner, B. Heim, C. Marquardt, G. Leuchs, R. W. Boyd, and E. Karimi, Optica **4**, 1006 (2017).
4. N. B. Simpson, L. Allen, and M. J. Padgett, J. Mod. Opt. **43**, 2485 (1996).
5. M. J. Padgett and R. Bowman, Nat. Photonics **5**, 343 (2011).
6. P. Senthilkumaran, Appl. Opt. **42**, 6314 (2003).
7. V. Lerner, D. Shwa, Y. Drori, and N. Katz, Opt. Lett. **37**, 4826 (2012).
8. M. Mirhosseini, O. S. Magaña-Loaiza, C. Chen, B. Rodenburg, M. Malik, and R. W. Boyd, Opt. Express **21**, 30196 (2013).
9. Z. Wang, Y. Yan, A. Arbabi, G. Xie, C. Liu, Z. Zhao, Y. Ren, L. Li, N. Ahed, A. J. Willner, E. Arbabi, A. Faraon, R. Bock, S. Ashrafi, M. Tur, and A. E. Willner, Opt. Lett. **42**, 2746 (2017).
10. T. H. Lu and Y. C. Wu, Opt. Express **21**, 28496 (2013).
11. T. D. Huang and T. H. Lu, Appl. Phys. B **124**, 72 (2018).
12. K. Sueda, G. Miyaji, N. Miyanaga, and M. Nakatsuka, Opt. Express **12**, 3548 (2004).
13. S. S. R. Oemrawsingh, J. A. W. van Houwelingen, E. R. Eliel, J. P. Woerdman, E. J. K. Verstegen, J. G. Kloosterboer, and G. W. 't Hooft, Appl. Opt. **43**, 688 (2004).
14. M. W. Beijersbergen, L. Allen, H. E. L. O. van der Veen, and J. P. Woerdman, Opt. Commun. **96**, 123 (1993).
15. G. Millione, T. A. Nguyen, J. Leach, D. A. Nolan, and R. R. Alfano, Opt. Lett. **40**, 4887 (2015).
16. G. Gibson, J. Courtial, M. J. Padgett, M. Vasnetsov, V. Pas'ko, S. M. Barnett, and S. Franke-Arnold, Opt. Express **12**, 5448 (2004).
17. M. Krenn, R. Fickler, M. Fink, J. Handsteiner, M. Malik, T. Scheidl, R. Ursin, and A. Zeillinger, New J. Phys. **16**, 113028 (2014).
18. F. Töppel, A. Aiello, C. Marquardt, E. Giacobino, and G. Leuchs, New J. Phys. **16**, 073019 (2014).
19. E. Yao, S. Franke-Arnold, J. Courtial, and M. J. Padgett, Opt. Express **14**, 13089 (2006).
20. D. N. Naik, N. A. Saad, D. N. Rao, and N. K. Viswanathan, Sci. Rep. **7**, 2395 (2017).
21. R. Liu, L. J. Kong, W. R. Qi, S. Y. Huang, Z. X. Wang, C. Tu, Y. Li, and H. T. Wang, Opt. Lett. **44**, 2382 (2019).
22. W. Ji, C. H. Lee, P. Chen, W. Hu, Y. Ming, L. Zhang, T. H. Lin, V. Chigrinov, and Y. Q. Lu, Sci. Rep. **6**, 25528 (2016).
23. E. Karimi, B. Piccirillo, E. Nagali, L. Marrucci, and E. Santamato, Appl. Phys. Lett. **94**, 231124 (2009).
24. S. Lou, Y. Zhou, Y. Yuan, T. Lin, F. Fan, X. Wang, H. Huang, and S. Wen, Opt. Express **27**, 8596 (2019).
25. L. Allen, J. Courtial, and M. J. Padgett, Phys. Rev. E **60**, 7497 (1999).
26. Y. C. Lin, T. H. Lu, K. F. Huang, and Y. F. Chen, Opt. Express **19**, 10293 (2011).
27. S. C. Chu, Y. T. Chen, K. F. Tsai, and K. Otsuka, Opt. Express **20**, 7128 (2012).